






# Active and Passive Lateral Earth Pressure on Retaining Walls with Broken Sloped Backfill Using Finite Element Limit Analysis

Ali Shafiee<sup>1</sup> (✉) , Alireza Eskandarinejad<sup>2</sup> , and Amir Hossein Shafiee<sup>3</sup> 

<sup>1</sup> California State Polytechnic University Pomona, Pomona, CA, USA  
ashafiee@cpp.edu

<sup>2</sup> Golestan University, Gorgan, Iran

<sup>3</sup> Shahid Chamran University of Ahvaz, Ahvaz, Iran

**Abstract.** Retaining walls with broken sloped backfill (RWBSB) are popular in North America in transportation projects. AASHTO (AASHTO LRFD Bridge Design Specifications, Customary U.S. Units. American Association of State Highway and Transportation Officials, 2020) suggests a limit equilibrium analysis to calculate lateral earth pressure on RWBSB. In this paper, we used upper bound (UB) and lower bound (LB) finite element limit analysis (FELA) under plane strain conditions to calculate active and passive earth pressures on RWBSB. The accuracy of the adopted numerical method is first verified against some simple cases of active and passive earth pressures in the literature. Using this validated numerical approach, a parametric study is further performed to calculate active and passive earth pressures on RWBSB. The influence of various parameters including backfill friction angle, soil-wall friction angle, slope inclination angle, and height of the broken slope on the active and passive earth pressures are systematically investigated and discussed.

**Keywords:** Finite Element Limit Analysis · Broken Sloped Backfill · Active Earth Pressure · Passive Earth Pressure

## 1 Introduction

Evaluation of active and passive lateral earth pressure on retaining walls under various conditions is recognized as one of the major stability problems in geotechnical engineering. The classical solutions of Coulomb [4] and Rankine [14] are still known as two valid benchmarks in this field. However, several analytical (e.g., [3, 12]), numerical (e.g., [7, 13]), and experimental studies (e.g., [6]) can be found in the literature that addressed lateral earth pressures on retaining walls. Retaining walls with broken sloped backfill (RWBSB) are popular in North America in transportation projects. AASHTO [1] suggests a limit equilibrium analysis to calculate lateral earth pressure on RWBSB. Terzaghi et al. [18] addressed active lateral earth pressure on the RWBSB for five different types of the soils ranging from coarse-grained soils with no fines to very soft clays, and organic silts with the backfill slope ranging from 1v:1.5h to 1v:6h using limit

equilibrium analysis. However, they did not clarify the soil and soil-wall friction angle corresponding to each soil type.

In the present paper, we incorporated upper bound and lower bound finite element limit analysis (FELA) to evaluate both active and passive lateral earth pressure on the RWBSB. The influence of various parameters including soil and soil-wall friction angle, and broken slope backfill angle and height on the lateral earth pressure are presented and discussed.

## 2 Identification of the Problem and Numerical Simulation

### 2.1 Problem Statement

The geometry of the plane strain problem of interest is shown in Fig. 1. The definition of the problem includes a retaining wall with broken sloped backfill (RWBSB). The retaining wall with a height of  $H$  is simply modeled by a vertical rigid weightless plate subjected to a load illustrating an active and a passive earth thrust on the wall. A uniform horizontal pressure of  $q$  (which is defined as a load multiplier) is applied to the wall with the direction to the left and right for the active and passive case, respectively. The backfill properties, with a unit weight of  $\gamma$  and a slope height of  $h$ , are governed by the Mohr-Coulomb failure criterion obeying the associated flow rule. The backfill material is assumed to be granular with no cohesion and various internal friction angles of 30, 35, 40, and 45 degrees. The soil-wall friction angle  $\delta$  is simulated by applying a reduction factor,  $r$ , with an interval magnitudes from 0 (i.e., perfectly smooth wall) to 1 (i.e., perfectly rough wall) to the interface between soil and wall in Optum G2 software [8]. The slope angle  $\beta$  of the backfill above the wall (demonstrated by slope inclination of equal to 1.5h:1v, 2h:1v, 3h:1v, and 6h:1v) is applied to the model. OPTUM G2 software is a limit analysis-based software that combines finite element method with lower bound and upper bound limit analysis to solve variety of foundation engineering and retaining walls problems. Optum G2 uses a second-order cone programming for numerical optimization.

In the present work, the active and passive earth pressure coefficients of retaining walls with broken sloped backfill under plane strain conditions were determined assuming a triangular pressure distribution on the wall as follows:

$$k_a \text{ and/or } k_p = \frac{q}{\frac{1}{2}\gamma H \cos\delta} \quad (1)$$

where  $k_a$  and  $k_p$  denote the active and passive earth pressure coefficient, respectively. The software evaluates the value of  $q$  and  $k_a$  and  $k_p$  are then calculated from Eq. (1).

There must be no intersection of the shear failure zone of the active and passive case to the right and the bottom boundaries. Thus, the problem domain sizes are selected to be large enough by having the horizontal length of bottom boundary and the distance from the wall bottom to the bottom boundary as to be equal to seven times of wall height ( $7H$ ) and twice of wall height ( $2H$ ), respectively. The bottom of the model is fixed in both vertical and horizontal directions, while the vertical boundaries are constrained horizontally. However, the surface boundary of the backfill is free. The vertical movement of the wall is restricted, whereas the wall horizontal movement is free.

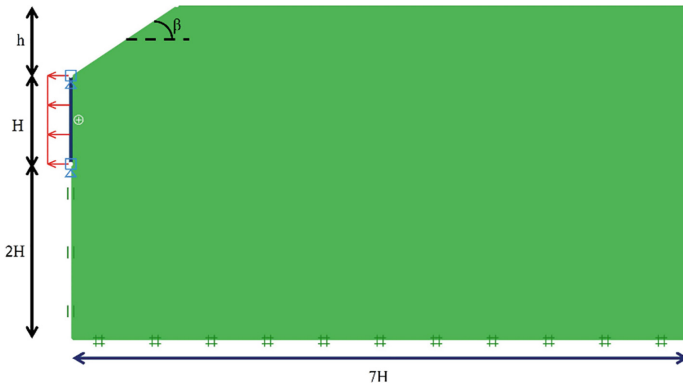


**Fig. 1.** Geometry of the model, boundary conditions, and loading under active earth pressure

## 2.2 Adaptive Finite Element Limit Analysis (AFELA)

An innovative tool of adaptive finite element limit analysis (AFELA) is employed here to determine the active and passive earth pressure coefficients for retaining walls with sloped backfills. Many researchers employed this technique to find the bracketed true collapse load for a wide variety of geotechnical problems [5, 9–11, 15–17]. This method can model the problems with complex failure geometries, loadings, and boundary conditions. The finite element discretization is utilized in AFELA for the problem medium assuming as a rigid-perfectly plastic material. In this study, solutions obtained by the two-dimensional lower bound (henceforth referred to as LB) and upper bound (henceforth referred to as UB) theorems of limit analysis is used to bracket the collapse load for retaining walls with sloped backfills. Numerical simulations were carried out by Optum G2 software. AFELA applies an automatic adaptive mesh refinement which is controlled by shear dissipation and effectively reduces the error. In numerical simulations, the initial number of elements was set to 5000 and increased to 15,000 after five stages of the automatic adaptive mesh refinement. It is worthy to mention that such a large number of elements has been applied after conducting a sensitivity analysis to limit relative worst-case errors ( $\frac{(UB-LB)}{(UB+LB)} \times 100$ ) within approximately 2.5%.

## 3 Validation

Figure 2 presents failure surface for a 5 m retaining wall with level ground,  $\phi = 40$  deg.,  $\delta/\phi = 2/3$  and  $\gamma = 19$  kN/m<sup>3</sup> under active (Fig. 2a) and passive (Fig. 2b) conditions predicted by upper bound AFELA. It is observed that the linear failure mechanism under the active case and logarithmic-spiral failure mechanism under passive case is consistent with the predicated failure mechanism by Coulomb and Caquot and Kerisel [2] for active and passive case respectively. Figure 3 also compares  $k_a$  and  $k_p$  from lower bound and upper bound AFELA for the same retaining wall when  $\delta/\phi$  varies from zero to one, against limit equilibrium-based Coulomb (for active case) and logarithmic-spiral (for passive case) approaches. It is observed that a good consistency exists amongst the results.

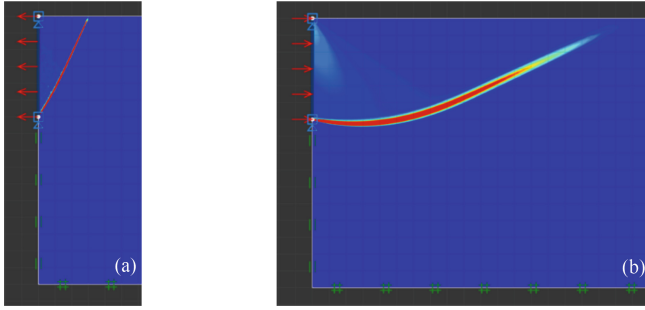


**Fig. 2.** Failure mechanism from upper bound AFELA under (a) active and (b) passive pressure

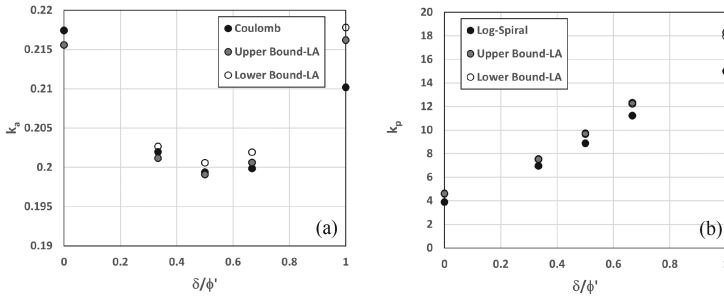


**Fig. 3.** Lateral earth pressure coefficient from AFELA versus (a) active case-Coulomb, and (b) passive case-logarithmic-spiral

We evaluated active earth pressure coefficient for RWBSB using limit equilibrium approach as well. Figure 4, for example, compares  $k_a$  from limit equilibrium against limit analysis when  $\phi = 30$  deg., and  $\delta/\phi = 1/3$  (Fig. 4a), and  $\delta/\phi = 2/3$  (Fig. 4b). The values of  $k_a$  for limit analysis were obtained by taking an average of the  $k_a$  from lower bound and  $k_a$  from upper bound a good consistency exists between the results.

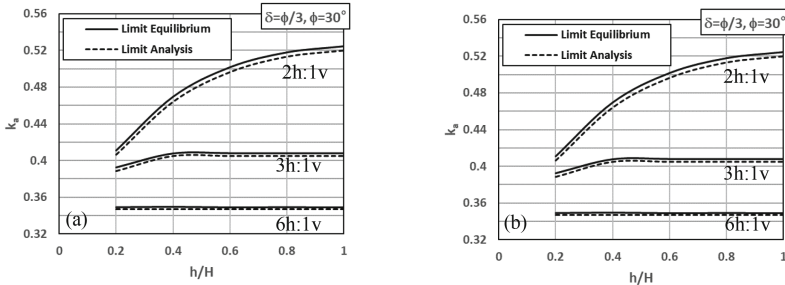


**Fig. 4.** Active lateral earth pressure coefficient from limit analysis versus limit equilibrium (a)  $\delta/\phi = 1/3$ , and (b)  $\delta/\phi = 2/3$

## 4 Active and Passive Earth Pressure Charts

We developed charts for both active (Fig. 5) and passive (Fig. 6) conditions for RWBSB under  $\gamma = 19 \text{ kN/m}^3$ ,  $H = 5 \text{ m}$ ,  $\phi = 30, 35, 40, 45 \text{ deg}$ ,  $\delta/\phi = 0, 1/3, 1/2, 2/3, 1$ , backfill slope = 1.5h:1v, 2h:1v, 3h:1v, 6h:1v, and  $h/H = 0.2, 0.4, 0.6, 0.8, 1$ . As it is expected,  $k_a$  decreases with  $\phi$ , while  $k_p$  increases with  $\phi$ . It is observed that both  $k_a$  and  $k_p$  increase, when backfill slope is increased. On the other hand,  $k_a$  decreases with  $\delta$  until  $\delta/\phi = 1/2$ , after which  $k_a$  increases with  $\delta$ . However,  $k_p$  always increases with increase in  $\delta$ . Both  $k_a$  and  $k_p$  increase with backfill height ratio  $h/H$  until a certain value after which  $k_a$  or  $k_p$  remain constant. In other words, if  $k_a$  and  $k_p$  are independent of  $h/H$ , then the failure surface passes through the sloping ground, otherwise it passes through the level ground.

As an example, for a retaining wall with  $H = 5 \text{ m}$ ,  $h = 1 \text{ m}$  ( $h/H = 0.4$ ),  $\delta/\phi = 2/3$ , backfill slope = 1.5h:1v, and soil properties of  $\phi = 40 \text{ deg}$ ., and  $\gamma = 122 \text{ kN/m}^3$ , from Fig. 5,  $k_a = 0.31$ , and hence: active force on the wall =  $0.5 \times 0.31 \times 122 \times 5^2 = 473 \text{ kN/m}$ . On the other hand, for the same wall  $k_p = 21.47$  (Fig. 6), and hence passive force on the wall =  $0.5 \times 21.47 \times 122 \times 5^2 = 32,742 \text{ kN/m}$ .

## 5 Conclusions

The lower bound and upper bound AFELA considering associated flow rule were used to provide charts for active earth pressure coefficient ( $k_a$ ) and passive earth pressure coefficient ( $k_p$ ) for rigid vertical retaining walls with broken sloped backfill (RWBSB). The influence of backfill friction angle ( $\phi$ ), soil-wall friction angle ( $\delta$ ), slope inclination angle ( $\beta$ ), and height of the broken slope ( $h$ ) on  $k_a$  and  $k_p$  were evaluated. It was shown that the results were consistent with literature for some special cases of lateral earth pressure on retaining walls under active and passive conditions. Based on the analyses performed in the present study, the following general remarks can be drawn:

- When  $\phi$  is increased  $k_a$  decreases and  $k_p$  increases.
- When  $\beta$  is increased  $k_a$  decreases and  $k_p$  increases.
- When  $\delta$  is increased  $k_p$  increases. On the other hand,  $k_a$  decreases with  $\delta$  until  $\delta/\phi = 1/2$ , after which  $k_a$  increases with  $\delta$ .
- If the failure surface behind the wall passes through the sloping ground, then  $k_a$  and  $k_p$  are independent of  $h$ , otherwise if the failure surface passes through the level ground,  $k_a$  and  $k_p$  increases with  $h$ .

The developed approach may also be adopted to evaluate the lateral earth pressure on the retaining walls with complex backfill topography, cohesive backfill, and seismic lateral loads.

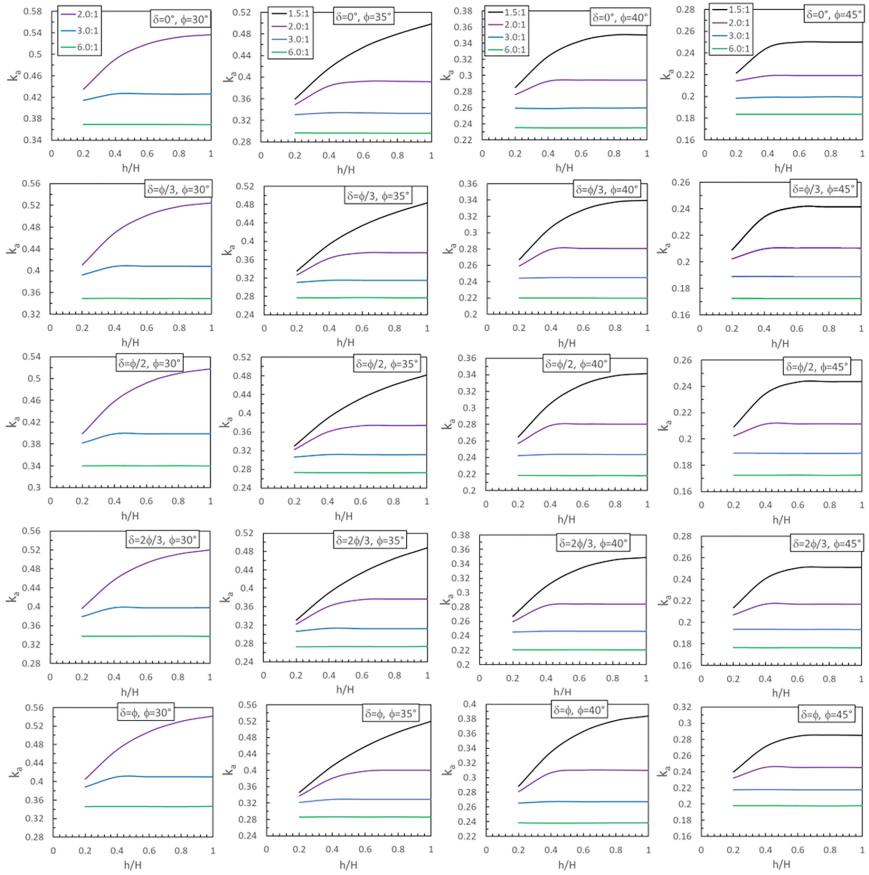


**Fig. 5.** Design charts for active lateral earth pressure coefficient of RWBSB

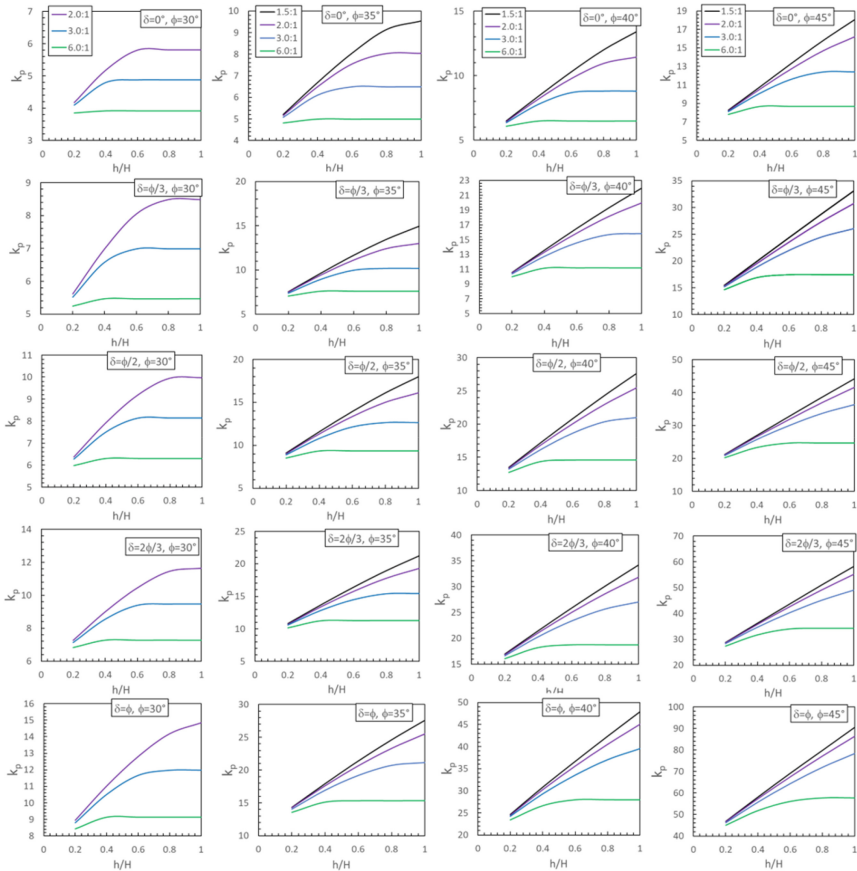


**Fig. 6.** Design charts for passive lateral earth pressure coefficient of RWBSB

## References

1. American Association of State Highway and Transportation Officials.: AASHTO LRFD Bridge Design Specifications, Customary U.S. Units. American Association of State Highway and Transportation Officials, (2020).
2. Caquot, A., Kerisel, J.: Tables for the calculation of passive pressure, active pressure and bearing capacity of foundations. Paris, France: Gauthier-Villars (1948).
3. Chen, W. F., Rosenfarb, J. L.: Limit analysis solutions of earth pressure problems. *Soils and Foundations* 13(4), 45–60 (1973).
4. Coulomb, C. A.: Essai sur une application des regles de maximis et minimis a quelques problemes de statique relatifs a l'architecture. *Mem. Div. Sav. Acad.* (1773).
5. Eskandarinejad, A.: Seismic vertical uplift capacity of horizontal strip anchors embedded in sand adjacent to slopes using finite element limit analysis. *Arabian Journal of Geosciences*, 15(1), p.16. (2022).
6. Fang, Y. S., Ho, Y. C., Chen, T. J.: Passive earth pressure with critical state concept. *Journal of Geotechnical and Geoenvironmental Engineering* 128(8), 651–659 (2002).

7. Fathipour, H., Safardoost Siahmazgi, A., Payan, M., Jamshidi Chenari, R., Veiskarami, M.: Evaluation of the active and passive Pseudo-dynamic earth pressures using finite element limit analysis and second-order cone programming. *Geotechnical and Geological Engineering* 41(2), 1–16 (2023).
8. Krabbenhoft, K., Lyamin, A.V., Krabbenhoft, J.: Optum computational engineering (OptumG2). <http://www.optumce.com> (2015).
9. Krabbenhoft, K.: Static and seismic earth pressure coefficients for vertical walls with horizontal backfill. *Soil Dyn Earthq Eng* 104:403–407 (2018).
10. Keawsawasvong, S., Ukritchon, B.: Undrained limiting pressure behind soil gaps in contiguous pile walls. *Comput Geotech* 83,152–158 (2017).
11. Lai, V.Q., Sangjinda, K., Keawsawasvong, S., Eskandarinejad, A., Chauhan, V.B., Sae-Long, W., Limkatanyu, S.: A machine learning regression approach for predicting the bearing capacity of a strip footing on rock mass under inclined and eccentric load. *Front. Built Environ.* 8:962331. doi: <https://doi.org/10.3389/fbuil.2022.962331> (2022).
12. Lin, Y. L., Yang, X., Yang, G. L., Li, Y., Zhao, L. H.: A closed-form solution for seismic passive earth pressure behind a retaining wall supporting cohesive–frictional backfill. *Acta Geotechnica* 12, 453–461 (2017).
13. Potts, D. M., Fourie, A. B.: A numerical study of the effects of wall deformation on earth pressures. *International journal for numerical and analytical methods in geomechanics*, 10(4), 383–405 (1986).
14. Rankine, W. J. M.: II. On the stability of loose earth. *Philosophical transactions of the Royal Society of London*, (147), 9–27 (1857).
15. Schmöderich, C., Alimardani Lavasan, A., Tschuchnigg, F., Wichtmann, T.: Behavior of nonidentical differently loaded interfering rough footings. *J Geotech Geoenv Eng* 146(6):04020041 (2020).
16. Shafiee, A.H., Eskandarinejad, A.: Bearing capacity of single stone column in clay using finite element limit analysis. *European Journal of Environmental and Civil Engineering*, 26(15), 7958–7971 (2022).
17. Sirimontree, S., Jearsiripongkul, T., Lai, V.Q., Eskandarinejad, A., Lawongkerd, J., See-havong, S., Thongchom, C., Nuaklong, P., Keawsawasvong, S.: Prediction of Penetration Resistance of a Spherical Penetrometer in Clay Using Multivariate Adaptive Regression Splines Model. *Sustainability* 2022, 14, 3222. <https://doi.org/10.3390/su14063222> (2022).
18. Terzaghi, K., Peck, R.B. and Mesri, G.: *Soil Mechanics in Engineering Practice*. 3rd Edition, John Wiley and Sons, Inc., New York (1996).

**Open Access** This chapter is licensed under the terms of the Creative Commons Attribution-NonCommercial 4.0 International License (<http://creativecommons.org/licenses/by-nc/4.0/>), which permits any noncommercial use, sharing, adaptation, distribution and reproduction in any medium or format, as long as you give appropriate credit to the original author(s) and the source, provide a link to the Creative Commons license and indicate if changes were made.

The images or other third party material in this chapter are included in the chapter’s Creative Commons license, unless indicated otherwise in a credit line to the material. If material is not included in the chapter’s Creative Commons license and your intended use is not permitted by statutory regulation or exceeds the permitted use, you will need to obtain permission directly from the copyright holder.

